

## Numerical studies of collinear laser-assisted injection from a foil for plasma wakefield accelerators

T. C. Wilson 

*Scottish Universities Physics Alliance, Department of Physics,  
University of Strathclyde, Glasgow G4 0NG, United Kingdom  
and Cockcroft Institute, Sci-Tech Daresbury, Cheshire WA4 4AD, United Kingdom*

J. Farmer

*Max-Planck-Institut für Physik, Munich 85748, Germany*

A. Pukhov

*Institut für Theoretische Physik I, Universität Düsseldorf, Düsseldorf 40225, Germany*

Z.-M. Sheng

*Key Laboratory for Laser Plasmas (MoE) and School of Physics and Astronomy,  
Shanghai Jiao Tong University, Shanghai 200240, People's Republic of China  
and Collaborative Innovation Center of IFSA, Shanghai Jiao Tong University,  
Shanghai 200240, People's Republic of China*

B. Hidding

*Scottish Universities Physics Alliance, Department of Physics,  
University of Strathclyde, Glasgow G4 0NG, United Kingdom  
and Cockcroft Institute, Sci-Tech Daresbury, Cheshire WA4 4AD, United Kingdom*



(Received 19 January 2024; accepted 8 July 2024; published 29 July 2024)

We present a laser-assisted electron injection scheme for beam-driven plasma wakefield acceleration. The laser is collinear with the driver and triggers the injection of hot electrons into the plasma wake by interaction with a thin solid target. We present a baseline case using the AWAKE Run 2 parameters and then perform variations on key parameters to explore the scheme. It is found that the trapped witness electron charge may be tuned by altering laser parameters, with a strong dependence on the phase of the wake upon injection. Normalized emittance settles at the order of micrometres and varies with witness charge. The scheme is robust to misalignment, with a 1/10th plasma skin-depth offset (20  $\mu\text{m}$  for the AWAKE case) having a negligible effect on the final beam. The final beam quality is better than similar existing schemes, and several avenues for further optimization are indicated. The constraints on the AWAKE experiment are very specific, but the general principles of this mechanism can be applied to future beam-driven plasma wakefield accelerator experiments.

DOI: [10.1103/PhysRevAccelBeams.27.071301](https://doi.org/10.1103/PhysRevAccelBeams.27.071301)

### I. INTRODUCTION

The potential benefits of plasma-based acceleration over traditional radio frequency (rf) acceleration are by now well documented. The high accelerating gradients possible in plasma make the scheme attractive for high-energy, low-emittance, and high-brightness beams from

very compact accelerators [1]. While originally envisioned as laser driven [2], the physics of plasma wakefields is mostly independent of the specific driver used, and particle beams may also be employed [1,3]. This has led to many advanced and hybrid schemes of laser and particle beam-driven accelerator concepts [4], in particular, proton beam-driven accelerators [5].

In any accelerator, a key metric by which it may be evaluated is the maximum obtainable energy. While in principle, this is simply the product of the accelerating gradient and length of the accelerator, plasma-based accelerators, in particular, are subject to two considerations that ultimately decide the limits on a single stage of acceleration. These are dephasing and driver depletion.

---

*Published by the American Physical Society under the terms of the Creative Commons Attribution 4.0 International license. Further distribution of this work must maintain attribution to the author(s) and the published article's title, journal citation, and DOI.*

Dephasing is a limiting factor wherein the witness beam eventually finds itself traveling faster than the wake and slowly moves out of the accelerating phase, thus limiting the maximum energy. This is typically relevant for laser-driven accelerators, as the velocity of the wake matches the group velocity of the laser, which is always somewhat lower than the speed of light in vacuum,  $c$ . This becomes significant when the typical accelerator length in laser-driven plasma wakefield accelerators (LWFA) is on the centimeter scale. Particle beam drivers (PWFA) can obtain velocities much closer to  $c$  and have longer typical accelerator lengths, so dephasing is much less of an issue.

Particle beam drivers may sidestep the issue of dephasing but are still subject to driver depletion. Eventually, the driver will lose enough of its own energy that it can no longer drive a sufficient wake and the accelerating gradient collapses. This loss is incurred gradually over the course of propagation, and techniques exist to suppress this loss [6] due to dispersion.

Both of these limitations may be removed by employing staging [7], which effectively extends the acceleration length indefinitely. This brings with it more factors to consider as the witness gains energy with each stage. The alignment constraints between the driver and witness become progressively more stringent, with small misalignments between the driver and witness being increasingly detrimental to the beam quality.

A relativistic proton beam carries several orders of magnitude more energy than a typical electron beam, effectively eliminating driver depletion. The high mass of the proton also corresponds to less synchrotron radiation under acceleration. All of this makes them attractive candidates for plasma acceleration, however, proton beams are difficult to compress, with the available proton beam sources operating with bunch lengths much longer than the preferred plasma period.

AWAKE is a proof-of-concept accelerator employing a proton beam sourced from the super proton synchrotron (SPS) at CERN [8]. The SPS proton beam is long,  $\sigma_{p^+} = 7$  cm, and thus spans several hundred skin depths of  $n_e = 7 \times 10^{14}$  cm<sup>-3</sup> plasma. The driver excites a plasma wake which then interacts with the driver itself, leading to so-called resonant self-modulation of the proton beam via the transverse two-stream instability [9–11]. This modulation causes the beam to periodically focus and defocus, resulting in a train of microbunches on the plasma wavelength scale, during which time the phasefronts of the plasma wake shift position. This constant phase shift during modulation makes it undesirable to inject electrons early. Thus, in the proposed Run 2c, the experiment is to be organized into two stages, for modulation, and acceleration respectively [12]. The experimental setup of AWAKE Run 2c is two identical stages of 10 m of plasma, separated by a 1 m gap (it should be emphasized again that this still is a proof-of-concept experiment and not representative of a

final accelerator design). The driver self-modulates to saturation in the first stage and in the second stage, simulations show that the phase structure of the wake changes very little, offering much more stable accelerating properties. The electron witness beam will be injected via the gap to join the driver as it enters the second stage. The presence of the gap introduces a drop in the final accelerating wakefield strength due to driver defocusing between cells, and minimizing or optimizing around this drop is an area of active work.

In AWAKE Run 2c, a traditional rf electron gun will be used to generate the witness. This will provide the electrons with significant initial energy, necessitating tight control over the alignment between driver and witness beams [13]. This will be achieved by bending magnets placed in the gap [14]. It has been shown recently via numerical simulations, that AWAKE should be capable of trapping electrons with a very low initial energy ( $\sim 2$  MeV) [15], opening up the possibility for alternative injection schemes that may be more compact and thus allow for a shorter gap between cells. The alternate scheme proposed by Khudiakov and Pukhov [15] employs a laser impacting a solid target at at 45° incidence, with the sprayoff electrons caught and accelerated by the wake. In this work, we offer a related scheme with the solid target at normal incidence to the laser pulse, in which MeV energetic electrons are accelerated at the front of the target and emitted from the rear side of the target.

## II. MECHANISM

The mechanism of our scheme follows from the mechanism of direct laser acceleration of electrons in laser interaction with a thin foil [16,17] and that of target-normal sheath acceleration (TNSA) [18]. An intense laser is incident on a thin foil. The laser is reflected, accelerating electrons through the foil in the process. When there is no plasma present on the far side of the foil, these electrons cause a sheath field to form, which constrains the electrons while simultaneously accelerating ions over hydrodynamic timescales. In our case, there is a plasma present beyond the foil. This allows the hot electrons to more readily stream away from the foil due to the return current that the background plasma provides. A relativistic particle beam can easily pass through such a thin foil, and when timed such that it arrives ahead of the laser, the hot electrons may enter into a preformed wake and become trapped.

A schematic view is shown in Fig. 1, with the major components labeled. The driver arrives first in Fig. 1(a), moving left-to-right through the foil preplasma, the solid foil, and into the plasma where it excites a quasilinear wake. The laser trails the driver by some distance  $\delta z$ , seen in Fig. 1(b), and is reflected by the preplasma, generating a plume of hot electrons in the process. These electrons are accelerated through the foil, pictured in Fig. 1(c), and are injected into the wake at a phase determined by  $\delta z$ .

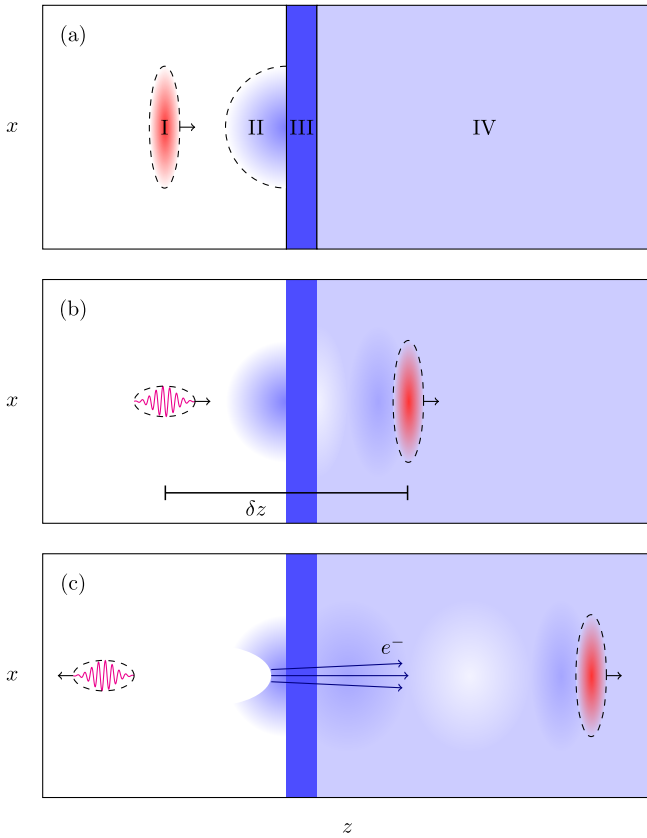


FIG. 1. Schematic view of the injection scheme. Initially (a) the driver (I) in vacuum, a preplasma (II) extending from a solid foil (III) with a preionized plasma (IV) on the far side. Once the driver has moved through the foil and into the plasma (b), the relativistic laser follows at a distance  $\delta z$ . The laser interacts with the preplasma and is reflected (c), producing hot electrons that stream through the foil and are captured by the wake set up by the driver.

We make the presumption that the foil will have a preplasma formed by the time the main pulse arrives. Such a preplasma is formed by the heating and subsequent ionization and thermal expansion of the front face of the foil either due to a combination of amplified spontaneous emission and laser prepulses ahead of the main pulse or by a dedicated ablation laser [19]. The foil in the immediate vicinity of the laser will necessarily be destroyed after each shot, and so for continuous operation, a system whereby the foil can be easily replaced is required. Disk-type targets offer such a solution in the  $< 1$  Hz repetition rate regime [20] by simply moving the target between shots such that fresh target material is in the path of the laser each time. If higher repetition rates are desired, tape drive targets could offer a solution of up to 100 Hz [21].

In experiment, the front face of the foil in the region of the laser will be ionized to a high level, with the electron density reaching on the order of  $\sim 100$  times the critical density. Such high densities are difficult to accurately model using particle-in-cell (PIC) codes, therefore as the

vast majority of injected electrons originate in the preplasma, we choose to exclude additional ionization in our simulation, instead making the assumption that the foil and preplasma are both fully ionized, with the foil density peaking only high enough to ensure the laser is reflected. As particles are pushed through the foil, the plasma is displaced and sheath fields will form on the far side until the plasma responds. These fields would cause additional ionization which is also excluded from our simulations. We also do not model any collisional effects, presuming that the driver beam is energetic enough that passing through a thin foil does not substantially affect it.

For a more complete modeling, these aforementioned effects should be considered. Further simulations using fluid or fluid-PIC hybrid codes may offer a richer view of the mechanisms.

The trapping conditions for particles injected into a quasilinear wake are derived in [15] from the Hamiltonian for the electron and consist of limits on the forward  $p_z$  and transverse  $p_r$  momentum relative to the wake. This condition takes the form

$$\frac{(p_z - p_c)^2}{a^2} + \frac{p_r^2}{b^2} < 1, \quad (1)$$

where  $p_z$ ,  $p_r$ , and  $p_c$  are all normalized to  $m_e c$ . This describes an ellipse in momentum space, offset from the origin by  $p_c$ , and with the principal axes described by the parameters  $a$  and  $b$ . The form of these parameters is as follows:

$$\begin{aligned} p_c &= \gamma_b^2 \beta_b T, \\ a^2 &= \gamma_b^2 (\gamma_b^2 T^2 - 1), \\ b^2 &= \gamma_b^2 T^2 - 1, \\ T &= \gamma_b^{-1} - \phi_0, \end{aligned}$$

where  $\gamma_b$  is the Lorentz factor of the drive beam,  $\beta_b = v_b/c$  is the normalized velocity of the drive beam, and  $\phi_0$  is the wakefield potential amplitude normalized to  $m_e c^2/e$  (plasma units). This condition is derived assuming particles are injected into the wake where the wake potential is minimized (the zero point of the longitudinal electric field), as this provides the most opportunity for a particle to be accelerated and subsequently captured before it falls backward out of the accelerating phase.

The exact delay required to inject into a given phase of the wake may be determined analytically or numerically. In the following simulations, we set the delay between the driver and laser such that the leading edge of the electron plume overlaps the zero point of the wake, i.e., where  $E_z = E_\perp = 0$ .

By nature, the plume of electrons pushed through the foil has very high charge and very high emittance overall. However, due to the aforementioned trapping conditions, self-selection occurs and particles with unfavorable

momentum or position quickly fall out of the wake and are lost. This results in a continuous reduction in charge and emittance over the first few centimeters of propagation until the beam stabilizes.

### III. SIMULATIONS

Simulations of the full SPS proton beam are extremely costly and inefficient for our purposes. Previous work has shown that with the AWAKE Run 2c setup, the wakefield in the acceleration stage will evolve very slowly. Therefore, a so-called toy model has been developed which mimics the AWAKE wakefield properties with a short rigid driver [22]. In addition, we employ a hybrid simulation setup, with the initial wake formation and laser interaction with the foil, being performed with the fully electromagnetic code FBPIC [23,24], and the latter acceleration performed with the quasistatic code QV3D [25].

The driver is Gaussian in shape, with  $\sigma_{z,p^+} = 40 \mu\text{m}$  and  $\sigma_{r,p^+} = 200 \mu\text{m}$ . The driver gamma factor is  $\gamma_0 = 427$ . The spot size and gamma factor are chosen to match the SPS beam, with the spot size corresponding to  $1/k_p$  for the AWAKE plasma density of  $n_e = 7 \times 10^{14} \text{ cm}^{-3}$ . The driver is modeled as randomly distributed macroparticles representing  $1.5 \times 10^{10}$  protons for a total charge of 2.4 nC, targeting a peak normalized wake potential of  $\phi_0 = 0.2$  and accelerating field of  $500 \text{ MV m}^{-1}$ . The driver does not evolve over the simulation.

The preplasma, foil, and bulk plasma are all initially cold. The foil is modeled as a preionized plasma of thickness  $L_{\text{foil}} = 50 \mu\text{m}$  and density  $n_{\text{foil}} = 3n_c$ , where  $n_c(\lambda_0)$  is the critical plasma density. The preplasma is modeled as half of a Gaussian ellipsoid extending from the surface of the foil with  $\sigma_{z,pp} = 5 \mu\text{m}$  and  $\sigma_{r,pp} = 10 \mu\text{m}$ . The preplasma density peaks at the critical density  $n_{pp} = n_c$ .

The laser has a vacuum wavelength of  $\lambda_0 = 800 \text{ nm}$ , a waist size of  $w_0 = 8 \mu\text{m}$ , duration  $\tau_0 = 20 \text{ fs}$ , and normalized amplitude  $a_0 = 2$ , corresponding to a total laser energy of  $W_l = 215 \text{ mJ}$ . The laser delay is informed by the trapping conditions and so to test this, we perform a scan of delay timings to verify this. The results are shown in Fig. 2, where we see confirmation that injection into the center of the wake provides both the maximum charge capture and the minimum emittance. The final bunch energy increases slightly when electrons are injected away from the wake, due to the reduction in beam loading. Energy spread also drops, but this is at the cost of much reduced final charge and poorer overall beam quality. In this way, we choose the laser to trail the driver by  $\delta z = 900 \mu\text{m}$ , a time delay of 3 ps.

## IV. RESULTS

### A. Baseline case

We may examine the accuracy of the trapping conditions by sampling the particles at different points of the

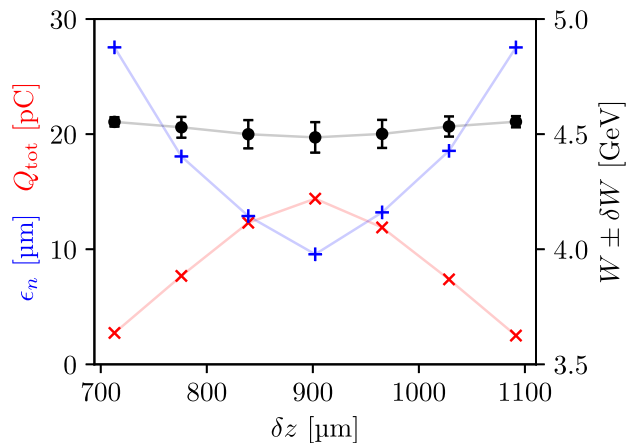


FIG. 2. A scan of final bunch properties plotted against the laser delay  $\delta z$ . A delay of  $\delta z \approx 900 \mu\text{m}$  corresponds to injecting into the center of the wake ( $E_z = 0$ ). The energy and energy spread (black, error bars), total charge (red), and emittance (blue) for several driver-laser delay timings are shown.

simulation. We plot the momentum space of all particles pushed through the foil in Fig. 3(a), with the particles located within the bounded expected to be trapped. Then, after 70 cm of propagation, we replot the initial momentum of the remaining particles in Fig. 3(b). We see that the trapping condition is well reproduced in terms of the cutoff values.

Applying the trapping condition (1) to the full sample of hot electrons using a value of  $\phi_0 = 0.195$  (calculated numerically), chosen to match the field value from the simulation, we retrieve the total expected trapped charge as 17.7 pC. We can then compare this to the remaining particles after 10 m to check the prediction. In this case, the actual trapped charge is 14.4 pC, a roughly 20% overestimation.

In practice, there is a spatial dependence on the trapping which is not captured by (1). Electrons that enter the wake away from the center are less easily trapped, as they have less distance to travel before falling out of the accelerating/focusing phase. This manifests in the analysis as a discrepancy between the predicted trapped charge, based on the initial particle distribution, and the actual trapped charge at the end of the simulations. It is therefore not surprising that the actual trapping will be lower than the prediction, as we assume ideal conditions for both the initial particle positions and the linearity of the wake.

As it happens, the spatial distribution of the electron plume can act to self-select particles with favorable positions, as those with the highest forward momentum will by nature all appear within a small volume at the head of the plume. The spatial distribution of the particles in the plume is shown in Fig. 3(c), and we have overlaid a bounded area corresponding to the physical locations of those particles expected to be trapped. As per Fig. 3(b), we also plot the initial positions of the final bunch of trapped

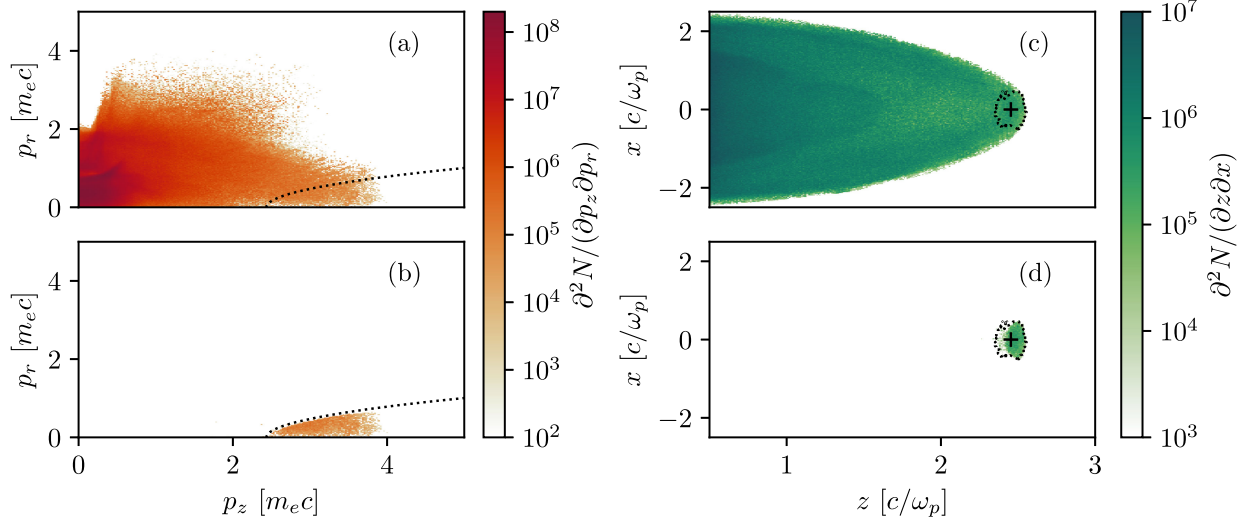


FIG. 3. Initial momentum (left) and position (right) of the hot electrons immediately upon entry to the plasma (top) and of those remaining after 70 cm (bottom). Particles within the bounded areas are those expected to be trapped. The plus denotes the zero point of the wake.

particles in Fig. 3(d), where we see that the particles with favorable momentum are also correlated in space. We see that they are indeed close to the zero point of the wake, denoted by the plus symbol. Thus, the spatial component of the trapping is often automatically satisfied for low  $\phi_0$ .

A summary of the key witness properties is shown in Fig. 4, with the final energy phase space shown in Fig. 4(a). After 10 m the witness has a mean energy of 4.5 GeV with relative energy spread of 1.5% (calculated as  $\sigma_{W_K}/\langle W_K \rangle$ ) and 8.5  $\mu\text{m}$  mean emittance.

The energy evolution is shown in Fig. 4(b), and the emittance evolution in Fig. 4(c), where we use a log scale to

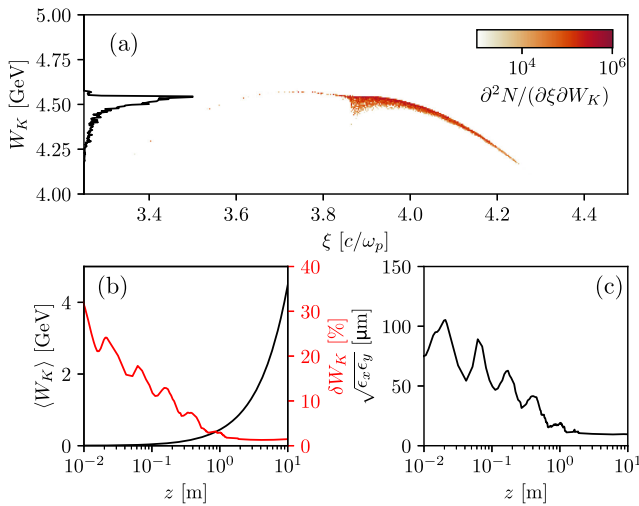


FIG. 4. Summary of the witness evolution. (a) Witness bunch energy-position phase space after 10 m, and energy spectrum (left). (b) Mean energy (black) and energy spread (red) evolution over the 10 m. (c) Average (geometric mean) normalized emittance.

highlight the rapid evolution the witness undergoes in the early stages of the acceleration. Around 50 nC of charge is pushed through the foil, but as we see from Fig. 3, the vast majority of the particles fall well outside the trapping region, and the charge is rapidly lost within the first centimeters of propagation. A prominent feature in the energy spread and emittance evolution is several large oscillations in the overall bunch properties with a decaying frequency (note again the log scale). These modulations are due to the betatron oscillations of the bunch. In the early stages, before phase mixing can occur, the bunch undergoes these oscillations semicoherently, causing the macroscopic properties of the bunch to fluctuate in turn. The continual loss of particles during this time also causes an apparent reduction in overall emittance and energy spread. Once all the particles that cannot be trapped are lost, and the bunch properties settle after about a meter.

## B. Additional simulations

Additional simulations were then performed to explore some of the properties and scaling relations for this scheme. In order to study the effect of a misalignment between the driver and the witness, a simulation was performed where the imported particles to QV3D were shifted by 20  $\mu\text{m}$ . The results of this simulation were very similar to the baseline case, with a final energy of  $4.5 \pm 1.5\%$  GeV and slightly increased 10.3  $\mu\text{m}$  emittance. The final witness charge was 14.0 pC, again only slightly worse than the baseline. This result suggests a high tolerance for misalignment. This is likely due to the fact that the particles are essentially accelerated from rest, so a small misalignment at such an early stage has little effect. We do not consider a pointing misalignment, however, as the particles are essentially

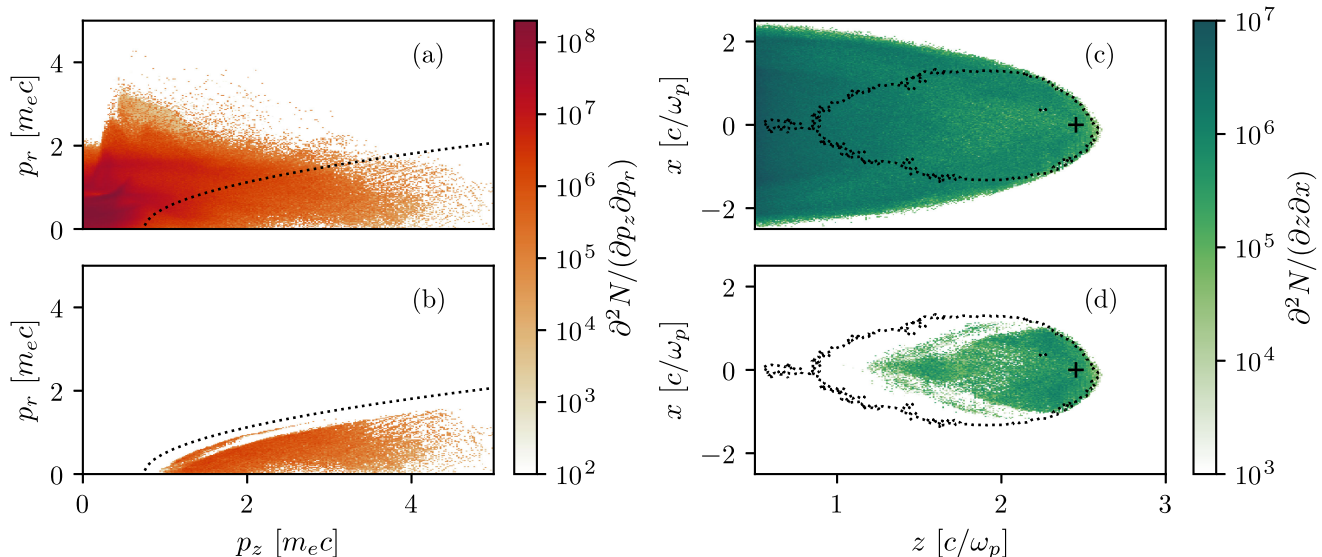


FIG. 5. Initial momentum (left) and position (right) of the hot electrons immediately upon entry to the plasma (top), and of those remaining after 30 cm (bottom). The bounded areas show particles that are expected to be trapped given  $\phi_0 = 0.5$ . The plus denotes the zero point of the wake.

accelerated from rest, we expect this to have a similarly small impact.

We also study the effect of preplasma length by running a simulation with a double-length preplasma where  $\sigma_{z,pp} = 10 \mu\text{m}$ . Keeping all other parameters the same, we find that the final charge of the witness is increased to 36.4 pC, suggesting doubling the scale of the preplasma more than doubles the captured charge. The beam energy is slightly reduced at  $4.34 \pm 1.8\%$  GeV, in-line with the slightly increased beam loading the heavier witness induces. Emittance is similarly higher at  $12.5 \mu\text{m}$ , again due to the higher charge.

Finally, the effect of the wakefield will have a substantial effect on the final witness, in terms of both the charge capture and the final energy. A much stronger wakefield with  $\phi_0 = 0.5$  was simulated, resulting in radically different bunch properties. This represents a somewhat extreme case, with the total final charge capture over an order of magnitude higher at 518 pC and a nearly doubled final energy of  $8.5 \pm 6\%$  GeV. Due to the much higher charge, the emittance is increased compared to the previous results to  $30.9 \mu\text{m}$ .

As the injection of the witness is dependent on the conditions of the plasma as it enters, we reran the initial simulation including the stronger wake. The trapping expectations and results are shown in Fig. 5. When compared to Fig. 3, there is an immediate different visible in the momentum distribution of the particles. We expect the laser-solid interaction to be decoupled from the later plasma wakefield properties, however, the momentum distribution in Fig. 5(a) is noticeably more elongated along  $p_z$ , with particles reaching higher forward momentum. The cause of this is not immediately clear and may indicate that

the properties of the hot plume of electrons are sensitive to the condition of the plasma close to the foil upon their entry to the plasma. This indicates that further study centered on the very early stages of laser-solid interaction is necessary to properly understand the injection process.

As expected, a stronger wake allows us to trap many more particles, spread over a much larger volume as indicated in Figs. 5(a) and 5(c). A total of 1682 pC is predicted to be trapped, based on summing all particles within the trapped region in Fig. 5(a). The simulation gives an aforementioned final witness charge of 518 pC, 30% of the prediction. This is again a result of the spatial dependence of the trapping. Figure 5(d) shows these spatial effects very clearly, with the predicted trapping volume overlaying the initial positions of the trapped particles. The particles are clustered around the midpoint of the wake, indicated by the plus, but particles too far from this point are lost. The trapped particles form a rough ellipse around the center of the wake, cut off by the leading edge of the plume. We postulate that in this specific case, it may be possible to increase the charge capture by shortening the delay between the driver and the laser such that the plume enters the wake with the midpoint further back, thus maximizing the number of particles with both favorable momentum and favorable position.

## V. CONCLUSION

We have successfully demonstrated the numerical simulation of collinear laser-assisted injection into a (quasilinear) plasma wakefield. A relativistic laser of modest energy may be employed to generate a plume of hot electrons from a foil preplasma. The properties of the

plume are tunable based on the choice of laser parameters and preplasma profile. Particles from this plume may then be captured and accelerated by a plasma wakefield, resulting in a higher-quality beam than that produced by the scheme of oblique-incidence laser-solid interaction [15]. The final beams show energy spread in the  $< 10\%$  range and emittances of the order of  $10 \mu\text{m}$ . Such emittances are suitable for fixed-target experiments and with optimization may yet be reduced further.

Our work has indicated several possible routes for further study and optimization of the scheme. The conditions of the plasma close to the foil strongly affect the charge entering the plasma, and the preplasma profile affects the total charge of the hot electron plume. In addition, the laser is at normal incidence to the target in our simulations, while in real experiments, the laser may be incident with certain angles. All of these aspects bear further investigation. Temperature effects and ionization of the foil were deliberately excluded in this study, so these aspects should be included in future work for a more rigorous evaluation. Additional aspects for consideration include the interaction of the laser with the preplasma before reflection and the thickness and material of the foil itself. This scheme offers a novel injection scheme that could greatly reduce the size and cost of external injection for plasma-wakefield acceleration.

#### ACKNOWLEDGMENTS

The authors acknowledge the United Kingdom Science and Technology Facilities Council Grants No. ST/V001612/1, No. ST/T00195X/1, and No. ST/X006298/1. This work used computational resources of the National Energy Research Scientific Computing Center, which is supported by DOE DE-AC02-05CH11231.

- 
- [1] M. Litos *et al.*, 9 GeV energy gain in a beam-driven plasma wakefield accelerator, *Plasma Phys. Controlled Fusion* **58**, 034017 (2016).
  - [2] T. Tajima and J. M. Dawson, Laser electron accelerator, *Phys. Rev. Lett.* **43**, 267 (1979).
  - [3] P. Chen, J. M. Dawson, R. W. Huff, and T. Katsouleas, Acceleration of electrons by the interaction of a bunched electron beam with a plasma, *Phys. Rev. Lett.* **54**, 693 (1985).
  - [4] A. F. Habib *et al.*, Plasma photocathods, *Ann. Phys. (Berlin)* **535**, 2200655 (2023).
  - [5] A. Caldwell *et al.*, Proton-driven plasma-wakefield acceleration, *Nat. Phys.* **5**, 363 (2005).
  - [6] A. Pukhov and J. P. Farmer, Stable particle acceleration in coaxial plasma channels, *Phys. Rev. Lett.* **121**, 264801 (2018).

- [7] C. A. Lindström, Staging of plasma-wakefield accelerators, *Phys. Rev. Accel. Beams* **24**, 014801 (2021).
- [8] E. Gschwendtner *et al.*, AWAKE, the advanced proton driven plasma wakefield acceleration experiment at CERN, *Nucl. Instrum. Methods Phys. Res., Sect. A* **829**, 76 (2016).
- [9] N. Kumar, A. Pukhov, and K. Lotov, Self-modulation instability of a long proton bunch in plasmas, *Phys. Rev. Lett.* **104**, 255003 (2010).
- [10] B. Allen, V. Yakimenko, M. Babzien, M. Fedurin, K. Kusche, and P. Muggli, Experimental study of current filamentation instability, *Phys. Rev. Lett.* **109**, 185007 (2012).
- [11] AWAKE Collaboration, Experimental observation of proton bunch modulation in a plasma, at varying plasma densities, *Phys. Rev. Lett.* **122**, 054802 (2018).
- [12] E. Gschwendtner *et al.*, The AWAKE Run 2 programme and beyond, *Symmetry* **14**, 1680 (2022).
- [13] J. P. Farmer *et al.*, Injection tolerances and self-matching in a quasilinear wakefield accelerator, [arXiv:2203.11622](https://arxiv.org/abs/2203.11622).
- [14] R. Ramjiawan, V. Bencini, P. N. Burrows, and F. M. Velotti, Design of the proton and electron transfer lines for AWAKE run 2c, *Nucl. Instrum. Methods Phys. Res., Sect. A* **1049**, 168094 (2023).
- [15] V. Khudiakov and A. Pukhov, Optimized laser-assisted electron injection into a quasilinear plasma wakefield, *Phys. Rev. E* **105**, 035201 (2022).
- [16] S. C. Wilks, W. L. Kruer, M. Tabak, and A. B. Langdon, Absorption of ultra-intense laser pulses, *Phys. Rev. Lett.* **69**, 1383 (1992).
- [17] A. Pukhov, Z.-M. Sheng, and J. Meyer-ter-Vehn, Particle acceleration in relativistic laser channels, *Phys. Plasmas* **6**, 2847 (1999).
- [18] A. Macchi, Ion acceleration by superintense laser-plasma interaction, *Rev. Mod. Phys.* **85**, 751 (2013).
- [19] P. McKenna *et al.*, Effects of front surface plasma expansion on proton acceleration in ultraintense laser irradiation of foil targets, *Laser Part. Beams* **26**, 591 (2008).
- [20] Y. Gao *et al.*, An automated, 0.5 Hz nano-foil target positioning system for intense laser plasma experiments, *High Power Laser Sci. Eng.* **5**, e12 (2017).
- [21] N. Xu *et al.*, Versatile tape-drive target for high-repetition-rate laser-driven proton acceleration, *High Power Laser Sci. Eng.* **11**, e23 (2023).
- [22] V. K. Berglyd Olsen, E. Adli, and P. Muggli, Emittance preservation of an electron beam in a loaded quasilinear plasma wakefield, *Phys. Rev. Accel. Beams* **21**, 011301 (2018).
- [23] R. Lehe, M. Kirchen, I. A. Andriyash, B. B. Godfrey, and J.-L. Vay, A spectral, quasi-cylindrical and dispersion-free particle-in-cell algorithm, *Comput. Phys. Commun.* **203**, 66 (2016).
- [24] FBPIC documentation. <https://fbpic.github.io/index.html> [accessed November 7, 2023].
- [25] A. Pukhov, Particle-in-cell codes for plasma-based particle acceleration, CERN Yellow Reports, 1:181, 2016, <https://doi.org/10.5170/CERN-2016-001.181>.